THE JOURNAL OF PHYSICAL CHEMISTRY Letters

Letter

pubs.acs.org/JPCL

Elucidation of $CuWO_4$ Surface States During Photoelectrochemical Water Oxidation

Yuan Gao and Thomas W. Hamann*

Department of Chemistry, Michigan State University 578 South Shaw Lane, East Lansing, Michigan 48824-1322, United States

Supporting Information

ABSTRACT: Electrochemical, photoelectrochemical, and impedance spectroscopy measurements were performed to investigate the role of $CuWO_4$ surface states during water oxidation. We found that a capacitive feature related to a surface state is clearly observable under water oxidation conditions. The magnitude of the surface state capacitance is light intensity-dependent, with a peak potential that coincides with the water oxidation onset potential region. The surface state is not observed in the dark nor in contact with nonaqueous solvents. These results strongly support our assignment of this surface state as the buildup of water oxidation intermediate species at the surface of $CuWO_4$ photoanodes, not a permanent or intrinsic state as previously reported. We suggest this is a general feature that controls the behavior and efficiency of solar water splitting reactions.

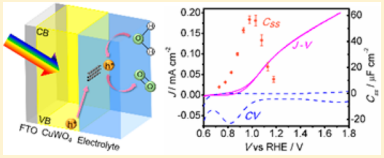

An increasing global demand for energy combined with concerns of climate change motivates more effective utilization of solar energy as an alternative of fossil fuels.[1−3] Photoelectrochemical water splitting, where semiconductors harness solar photons to generate hydrogen, provides an attractive route to convert and store solar energy in a clean and renewable secondary energy source.[4−7] Suitable semiconductors to drive the photoelectrochemical (PEC) oxygen evolution reaction (OER) must have a bandgap small enough to allow absorption of a significant portion of the visible part of sunlight and a valence band position capable of providing sufficient overpotential to drive the OER reaction. Ideally, the semiconductor should be composed of earth abundant elements and be stable in aqueous electrolytes under water splitting conditions.[4] In addition, the photogenerated holes should be effectively separated and collected selectively via the OER reaction at the electrode surface. Metal oxides are an attractive class of materials since they are generally stable with valence band positions capable of driving the OER. While binary oxides such as TiO_2, Fe_2O_3, WO_3, etc. have long been studied as water oxidation photoanodes,[5,8−13] ternary and quaternary oxides have attracted emerging interest recently because of their diversity and tunability.[14−22]

Copper tungstate ($CuWO_4$) is one of the most promising photoanodes due to its reasonably small band gap (2.3 eV), stability in neutral and slightly basic solutions under water oxidation conditions and earth abundant composition.[14,23−27] While the bandgap of $CuWO_4$ allows a photocurrent density up to ∼9 mA cm^{-2} to be produced, the best photocurrents achieved to date is only ∼0.3 mA cm^{-2}.[28] In addition, the photocurrent onset potential is several hundred millivolts positive of the flat band potential. Such poor PEC performance has been attributed to both limited charge separation and hole collection efficiencies.[26,27,29,30] To overcome the opposing properties of a long light absorption depth[25,27] and poor charge separation efficiency, strategies such as nanostructuring[31,32] and doping[30] have been pursued. Prior reports have also suggested the hole collection efficiency is low, due to slow water oxidation kinetics and the presence of a midgap surface state which mediates the OER on $CuWO_4$.[26,29,30,33]

We recently determined that the hole collection efficiency is actually quantitative at potentials higher than 1.23 V vs RHE.[34] This finding required use of Na_2SO_3 as a suitable sacrificial hole scavenger, whereas we found that H_2O_2 gives rise to current multiplication with $CuWO_4$.[30] Thus, poor hole collection via water oxidation with $CuWO_4$ only occurs in the low potential region, indicated the photocurrent onset potential. Interestingly, there is only one report to date that has investigated the nature of the surface states of $CuWO_4$, where it was concluded to be an intrinsic state.[29] This interpretation is different from what we have now established with hematite electrodes, where a surface state develops as a water oxidation intermediate species.[35−38] In this work, we aim to reconcile the nature of surface states on $CuWO_4$ and better understand water oxidation on semiconductors in general.

The $J_{photo}-V$ curves of $CuWO_4$ in contact with H_2O and with a sacrificial hole scavenger, Na_2SO_3, are compared in Figure 1. The raw data of $J_{total}-V$ and $J_{dark}-V$ are shown in Figure S1. Na_2SO_3 has been shown to be a suitable sacrificial hole scavenger which produces quantitative hole collection with $CuWO_4$.[34] The photocurrent onset potential of water oxidation is ∼0.85 V vs RHE. When Na_2SO_3 is in the electrolyte, however, the onset potential is shifted negatively to 0.6 V vs RHE. The discrepancy in the onset potential, as well as the photocurrent in the onset potential region, between water oxidation and oxidation of Na_2SO_3 is due to inefficient hole collection via water oxidation at the $CuWO_4$ surface.[34]

EIS measurements were performed on nominally identical $CuWO_4$ electrodes in contact with H_2O and Na_2SO_3

Received: March 20, 2017
Accepted: May 30, 2017
Published: June 6, 2017

DOI: 10.1021/acs.jpclett.7b00664
J. Phys. Chem. Lett. 2017, 8, 2700−2704

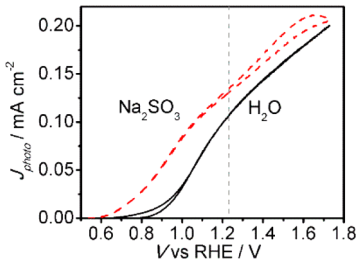

Figure 1. J_{photo}−V curves of a $CuWO_4$ electrode in contact with a pH 9.0 KB_i electrolyte in the absence (black solid curve) and presence (red dashed curve) of 0.5 M Na_2SO_3 under 1 sun illumination. The vertical gray dash represents the thermodynamic potential of water oxidation (1.23 V vs RHE).

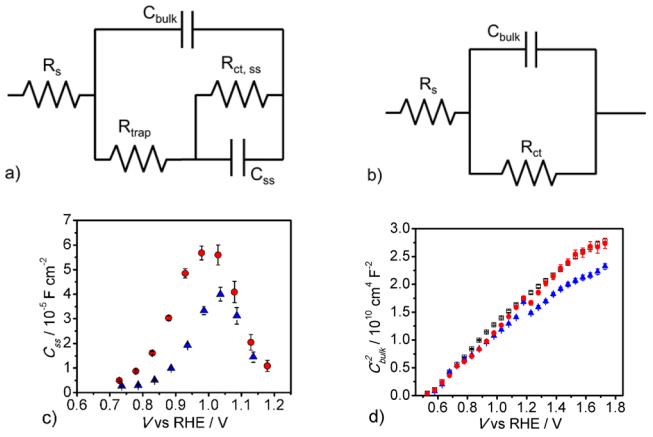

Figure 3. (a) Equivalent circuit for EIS data with two capacitive features. (b) Randle's circuit. (c) C_{ss} obtained from fitting EIS under 0.1 sun (blue triangles) and 1 sun (red circles) illumination in H_2O electrolyte. (d) Mott−Schottky plots of $CuWO_4$ immersed in aqueous electrolyte (H_2O), measured in the dark (open squares), under 0.1 sun (blue triangles) and 1 sun (red circles) illumination.

electrolytes to elucidate the processes that control the J−V behavior.[35] Figure 2 displays Bode plots, which indicate capacitive elements that appear in the EIS spectra. The Bode phase plots are presented instead of the Nyquist plots since in some cases the two semicircles are merged together; however, the corresponding Nyquist plots are shown in Figure S2. In the dark, the Bode phase plots show only one peak at all potentials, in contact with either H_2O or Na_2SO_3 electrolyte, which is assigned to the space charge capacitance. This suggests that the surface state capacitance is not observable in the dark at these potentials. Under 1 sun illumination, in the potential range of 0.68−1.23 V vs RHE, two capacitive peaks are clearly observed in the Bode phase plot for $CuWO_4$ electrodes immersed in the H_2O electrolyte; at higher potentials only one peak is seen. On the other hand, only one peak could be observed in the Na_2SO_3 electrolyte at all potentials under illumination.

The EIS data were fit to a model shown in Figure 3a, which includes the impedance from a surface state, which is adopted from the model established with hematite.[35,39] Here R_s represents the series resistance from the bulk of the semiconductor, electrical contacts, and electrolyte, C_{bulk} describes the bulk capacitance, which in this potential region is dominated by space charge capacitance, R_{trap} is the resistance of trapping of holes in the surface states. C_{ss} is the surface state capacitance, and $R_{ct,ss}$ describes the charge transfer resistance via the surface states. For EIS data in the dark and under illumination with only one capacitive feature, the Randle's circuit is used (Figure 3b).

Values of C_{ss} extracted from fitting EIS data to the equivalent circuits displayed in Figure 3a are plotted in Figure 3c. All other parameters derived from fits are shown in Figure S3. The only spectra that exhibited two capacitive features, as shown in Figure 2b, are measured under illumination with an H_2O electrolyte, i.e., under PEC water oxidation conditions. The magnitude of the fitted C_{ss} peak decreases when the light intensity is decreased from 1 sun to 0.1 sun. The peak in C_{ss} at ∼1.0 V vs RHE is associated with a dip in $R_{ct,ss}$ (Figure S3b), which is close to the water oxidation onset potential. The peak position of C_{ss} also matches the charge stored at the surface determined by integration of photocurrent transient measurements shown in Figure S5c. These results strongly support the assignment of this peak to a water oxidation intermediate species as opposed to an intrinsic state.

The fitted C_{bulk} values decrease with applied voltage, but are essentially invariant at a given potential in the dark and under different light intensities (Figure S3c). Mott−Schottky plots were constructed from C_{bulk} values, which are displayed in Figure 3d. The Mott−Schottky plots measured in the dark, under 0.1 sun and 1 sun conditions overlap with each other. The flat band potential (E_{fb}) of $CuWO_4$ was calculated to be 0.50 ± 0.02 V vs RHE, and the dopant density (N_d) is 6.3 ± 0.1 × 10^{19} cm^{-3} based on the data measured in the dark. The calculated results under different illumination conditions are compared in Table S1. This flat band potential is comparable to literature values of ∼0.42 V vs RHE.[25,26,40] Unlike prior reports by Bartlett's group,[29] no indication of Fermi level pinning is observed herein for $CuWO_4$ in contact with H_2O, nor with the hole scavenger, Na_2SO_3 (Figure S4).

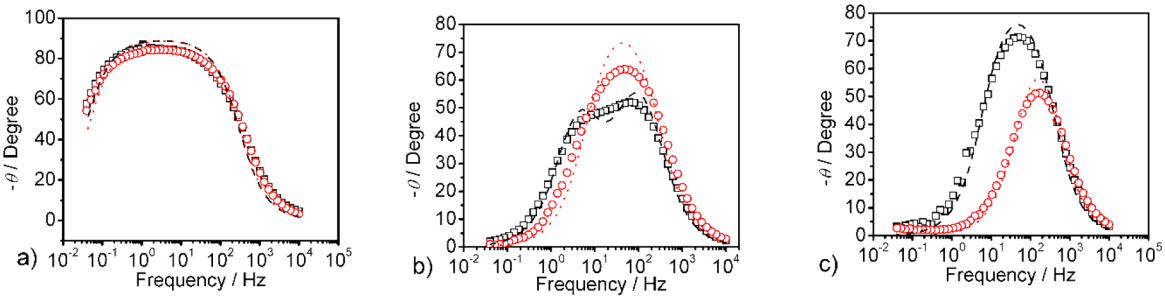

Figure 2. Bode phase plots of $CuWO_4$ electrode at 0.93 V vs RHE (a) in the dark and (b) under 1 sun illumination and (c) at 1.53 V vs RHE under 1 sun illumination. Data measured in H_2O (black squares) and 0.5 M Na_2SO_3 (red circles) are shown. Fitted curves are shown as black dashed lines for H_2O and red dotted lines for Na_2SO_3.

DOI: 10.1021/acs.jpclett.7b00664
J. Phys. Chem. Lett. 2017, 8, 2700−2704

Cyclic voltammetry (CV) was also utilized to examine the charging/discharging of the surface state.[41] A pretreatment of holding a positive potential of 2.3 V vs RHE either under illumination or in the dark for 60 s was performed, followed by a fast potential scan in the negative direction. We note this potential is sufficiently positive to oxidize the surface state even in the dark. As seen in Figure 4a and Figure S6, a cathodic peak

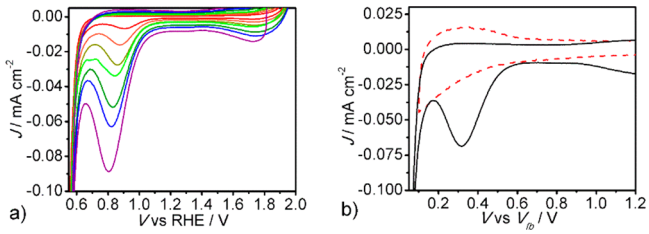

Figure 4. (a) CVs taken after holding potential at 2.3 V vs RHE for 60 s under 1 sun illumination at scan rates from 200, 400, 600, 800, 1000, 1200, and 1500 mV s^{-1} corresponding to red, orange, dark yellow, green, dark green, blue, and purple solid, respectively. (b) CV after holding potential at ∼1.8 V vs V_{fb} for 60 s in the dark, measured in H_2O (black solid) and MeCN (red dash). Scan rate is 1500 mV s^{-1}.

appears around 0.9 V vs RHE, indicating the reduction of the surface state, which is equivalent to recombination of surface-trapped holes with conduction band (CB) electrons. The intensity of the peaks increases with scan rate, which confirms the capacitive nature. The peak position is very close to the C_{ss} peak at 1.0 V vs RHE we observed in EIS measurements, as well as the peak position of the stored charge in current transient measurements, although in CV it is slightly shifted toward the negative potential due to the nonsteady state conditions at the fast scan rates. This further suggests that the peak of C_{ss} is associated with charging the surface state, which is related to water oxidation.

Analogous fast scan CVs were also performed in nonaqueous solvents, to determine whether the generated surface state is consistent with a water oxidation intermediate species. These experiments were conducted in a sealed electrochemical cell in the glovebox to minimize the influence of trace amounts of water. The CV curves measured in anhydrous acetonitrile (MeCN) are plotted vs V_{fb} of $CuWO_4$ measured in the same electrolyte (see Figure S7 for Mott−Schottky plots). No corresponding peak was observed even with fast scan rate (1500 mV s^{-1}) as shown in Figure 4b. We added 2% of H_2O to the MeCN electrolyte and conducted the same CV measurement. A small peak appeared at 0.4 V vs V_{fb}, which is the same potential where we observed a peak in aqueous electrolytes (Figure S8). Similar CV measurements were also performed in a noncoordinating solvent, dichloromethane, to eliminate the influence of any coordination of electrolyte species to the electrode surface. Figure S9 shows that no peak is under these conditions either. These results indicate that the surface state is available only in the presence of water, with sufficient applied bias or illumination to oxidize water, which confirms our argument that the surface state of $CuWO_4$ is related to water oxidation.

Electrodes prepared via ALD were utilized since this produces reproducible, uniform and compact films which allows a more straightforward interpretation of EIS data compared to nanostructured, porous films. Since differences in synthetic methods may potentially lead to different surface properties, we also carried out a complete set of control experiments with $CuWO_4$ synthesized via spray pyrolysis (SP-$CuWO_4$). The detailed synthetic method and results are provided in the SI. The C_{ss} obtained from fitting EIS data increased with increasing illumination intensity corresponding to 0.1, 0.33, and 1 sun, consistent with results discussed above of the ALD films. The Mott−Schottky plots of the SP-$CuWO_4$ in the dark show no indication of Fermi level pinning. Thus, in all cases, the electrodes prepared by SP behaved in nearly identical fashion as electrodes prepared by ALD. These combined results indicate that photogenerated surface states we observe for $CuWO_4$ is general to this material.

In conclusion, a surface state is clearly observed on $CuWO_4$ via several electrochemical methods. Importantly, we are only able to observe this state under water oxidation conditions, at a potential closely related to the water oxidation onset potential. These results strongly support an assignment of this surface state as a water oxidation intermediate species. This assignment contradicts prior reports who identified an intrinsic Cu-centered surface state.[29] Since the results did not depend on the synthetic method of preparing $CuWO_4$ electrodes, the assignment of the surface state to water oxidation intermediate species appears to be general for $CuWO_4$ photoanodes. It is also striking how similar $CuWO_4$ behaves compared to hematite, where it is established that a surface state arises from the first step of water oxidation. Recombination of this intermediate species with conduction band electrons gives rise to the shift in photocurrent onset potential since an additional potential needs to be applied to reduce surface electron concentration and thus recombination. Thus, the results presented here offer the first indication that this behavior of photoinduced surface state recombination is general for water oxidation with metal oxide semiconductors, which suggests a fundamental limitation to solar water splitting with bare electrodes. Addition of cocatalysts, such as Co-Pi or $NiFeO_x$ to the electrode surface, however, offers a route to circumvent this recombination path since photogenerated holes at the electrode surface can oxidize the catalyst preferentially to the electrode surface. Work is ongoing to elucidate the detailed charge transfer pathways and kinetics of the complex semiconductor/catalyst interface during water oxidation.

■ EXPERIMENTAL METHODS

Film Preparation. Copper tungstate ($CuWO_4$) thin films were deposited on fluorine-doped tin oxide (FTO)-coated glass (Hartford Glass, 12 Ω cm^{-2}) by an atomic layer stack deposition-annealing (SDA) method (Savannah 100, Cambridge Nanotech, Inc.) using a procedure described previously.[27] Briefly, 1000 cycles of WO_3 were deposited by atomic layer deposition (ALD), followed by ∼170 ALD cycles of CuO. After deposition, the stack of binary oxides was annealed at 550 °C in air for 30 min with a ramping rate of 2 °C/min. The thickness of the resulted $CuWO_4$ thin film was calculated to be ∼80 nm which agrees with the result from scanning electron microscopy (SEM) and atomic force microscopy (AFM) in our previous publication.[27] The experimental details of ALD of each binary oxide layer and measurement of WO_3 thickness are stated in Supporting Information (SI). The synthesis of $CuWO_4$ by spray pyrolysis for control experiments are also described in the SI.

Photoelectrochemical Measurements. $CuWO_4$ working electrodes were measured in a three-electrode system using high surface area platinum mesh as the counter electrode. A pH 9.0 1 M KB_i buffer with or without 0.5 M Na_2SO_3 was used as the

DOI: 10.1021/acs.jpclett.7b00664
J. Phys. Chem. Lett. 2017, 8, 2700−2704

aqueous electrolyte. A homemade "no leak" saturated Ag/AgCl electrode was used as a reference electrode. When in contact with a nonaqueous electrolyte, $Ag/AgNO_3$ was used as the reference electrode. The working electrodes were examined in contact with anhydrous MeCN or dichloromethane with 0.2 M $TBAPF_6$ as the supporting electrolyte. Current density−voltage ($J-V$) curves were measured using a scan rate of 20 mV s^{-1}. The white light source was a 450 W Xe arc lamp (Horiba Jobin Yvon). An AM 1.5 solar filter was used to simulate sunlight at 100 mW cm^{-2}. A neutral density filter was used to reduce the light intensity to 10 mW cm^{-2}. All photoelectrochemical measurements in aqueous solutions were performed by shining light on the $CuWO_4$ electrode through the electrolyte. Photocurrent densities (J_{photo}) were obtained by subtracting the dark current density (J_{dark}) from the total current density under illumination (J_{total}). Cyclic voltammogram (CV) surface state measurements were performed by applying a positive potential in the dark or under illumination for 60 s, and then scanning toward the cathodic direction over a potential range in the dark. EIS data were gathered using a 10 mV amplitude perturbation of between 10000 and 0.04 Hz in the dark or under illumination of 0.1 sun or 1 sun. Neutral density filters were used to adjust the intensity to 10 mW cm^{-2} (0.1 sun). Data were fitted using Zview software (Scribner Associates). Experimental details are described in the SI.

■ ASSOCIATED CONTENT

Supporting Information

The Supporting Information is available free of charge on the ACS Publications website at DOI: 10.1021/acs.jpclett.7b00664.

Experimental details, $J-V$ raw data, EIS raw data and fitted data, calculation of Mott−Schottky plots, photocurrent transient measurements, CV surface measurements under different conditions and measurement of V_{fb} in nonaqueous electrolytes (PDF)

■ AUTHOR INFORMATION

Corresponding Author

*E-mail: hamann@chemistry.msu.edu.

ORCID

Thomas W. Hamann: 0000-0001-6917-7494

Author Contributions

The experiments were designed by Y.G. and T.W.H. The experiments were carried out by YG. The manuscript was prepared by YG and TWH. All authors have given approval to the final version of the manuscript. The authors declare no competing financial interests.

Notes

The authors declare no competing financial interest.

■ ACKNOWLEDGMENTS

T.W.H. thanks the National Science Foundation (CHE-1150378) for support of this research.

■ REFERENCES

(1) Lewis, N. S.; Nocera, D. G. Powering the Planet: Chemical Challenges in Solar Energy Utilization. *Proc. Natl. Acad. Sci. U. S. A.* **2006**, *103*, 15729−15735.

(2) Gielen, D.; Boshell, F.; Saygin, D. Climate and Energy Challenges for Materials Science. *Nat. Mater.* **2016**, *15*, 117−120.

(3) Kerr, R. A. How Urgent Is Climate Change? *Science* **2007**, *318*, 1230−1231.

(4) Walter, M. G.; Warren, E. L.; McKone, J. R.; Boettcher, S. W.; Mi, Q.; Santori, E. A.; Lewis, N. S. Solar Water Splitting Cells. *Chem. Rev.* **2010**, *110*, 6446−6473.

(5) Fujishima, A.; Honda, K. Electrochemical Photolysis of Water at a Semiconductor Electrode. *Nature* **1972**, *238*, 37−38.

(6) Grätzel, M. Photoelectrochemical Cells. *Nature* **2001**, *414*, 338−344.

(7) Gust, D.; Moore, T. A.; Moore, A. L. Solar Fuels via Artificial Photosynthesis. *Acc. Chem. Res.* **2009**, *42*, 1890−1898.

(8) Klahr, B. M.; Martinson, A. B. F.; Hamann, T. W. Photoelectrochemical Investigation of Ultrathin Film Iron Oxide Solar Cells Prepared by Atomic Layer Deposition. *Langmuir* **2011**, *27*, 461−468.

(9) Liu, R.; Lin, Y.; Chou, L. Y.; Sheehan, S. W.; He, W.; Zhang, F.; Hou, H. J. M.; Wang, D. Water Splitting by Tungsten Oxide Prepared by Atomic Layer Deposition and Decorated with an Oxygen-Evolving Catalyst. *Angew. Chem., Int. Ed.* **2011**, *50*, 499−502.

(10) Dotan, H.; Sivula, K.; Gratzel, M.; Rothschild, A.; Warren, S. C. Probing the Photoelectrochemical Properties of Hematite (α-Fe_2O_3) Electrodes Using Hydrogen Peroxide as a Hole Scavenger. *Energy Environ. Sci.* **2011**, *4*, 958−964.

(11) Steier, L.; Herraiz-Cardona, I.; Gimenez, S.; Fabregat-Santiago, F.; Bisquert, J.; Tilley, S. D.; Grätzel, M. Understanding the Role of Underlayers and Overlayers in Thin Film Hematite Photoanodes. *Adv. Funct. Mater.* **2014**, *24*, 7681−7688.

(12) Mi, Q.; Zhanaidarova, A.; Brunschwig, B. S.; Gray, H. B.; Lewis, N. S. A Quantitative Assessment of the Competition between Water and Anion Oxidation at WO_3 Photoanodes in Acidic Aqueous Electrolytes. *Energy Environ. Sci.* **2012**, *5*, 5694.

(13) Hill, J.; Choi, K. Effect of Electrolytes on the Selectivity and Stability of n-Type WO_3 Photoelectrodes for Use in Solar Water Oxidation. *J. Phys. Chem. C* **2012**, *116*, 7612−7620.

(14) Benko, F. A.; MacLaurin, C. L.; Koffyberg, F. P. $CuWO_4$ and Cu_3WO_6 as Anodes for the Photoelectrolysis of Water. *Mater. Res. Bull.* **1982**, *17*, 133−136.

(15) Park, Y.; McDonald, K. J.; Choi, K.-S. Progress in Bismuth Vanadate Photoanodes for Use in Solar Water Oxidation. *Chem. Soc. Rev.* **2013**, *42*, 2321−2337.

(16) Guo, W.; Chemelewski, W. D.; Mabayoje, O.; Xiao, P.; Zhang, Y.; Mullins, C. B. Synthesis and Characterization of CuV_2O_6 and $Cu_2V_2O_7$: Two Photoanode Candidates for Photoelectrochemical Water Oxidation. *J. Phys. Chem. C* **2015**, *119*, 27220−27227.

(17) Murakami, Y.; Ikarashi, M.; Hashizume, M.; Nosaka, A. Y.; Nosaka, Y. Laser Ablation of the Photocatalytic $BiVO_4$ and $BiZn_2VO_6$ Powders in Water and Their Photocurrent Properties. *Electrochem. Solid-State Lett.* **2008**, *11*, H42−H46.

(18) Yu, J.; Zhang, Y.; Gao, X.; Kudo, A.; Zhao, X. S. Enhancement of Photo-to-Current Efficiency over Two-Dimensional Bi_2MoO_6 Nanoplate Thin-Film Photoelectrode. *Electrochem. Solid-State Lett.* **2008**, *11*, B197−B200.

(19) Kozuka, H.; Kajimura, M. Sol-Gel Preparation and Photoelectrochemical Properties of Fe_2TiO_5 Thin Films. *J. Sol-Gel Sci. Technol.* **2001**, *22*, 125−132.

(20) Joshi, U. A.; Jang, J. S.; Borse, P. H.; Lee, J. S. Microwave Synthesis of Single-Crystalline Perovskite $BiFeO_3$ Nanocubes for Photoelectrode and Photocatalytic Applications. *Appl. Phys. Lett.* **2008**, *92*, 242106.

(21) Zhao, X.; Wu, Y.; Yao, W.; Zhu, Y. Photoelectrochemical Properties of Thin Bi_2WO_6 Films. *Thin Solid Films* **2007**, *515*, 4753−4757.

(22) Tang, D.; Rettie, A. J. E.; Mabayoje, O.; Wygant, B. R.; et al. Facile Growth of Porous $Fe_2V_4O_{13}$ Films for Photoelectrochemical Water Oxidation. *J. Mater. Chem. A* **2016**, *4*, 3034−3042.

(23) Montini, T.; Gombac, V.; Hameed, A.; Felisari, L.; Adami, G.; Fornasiero, P. Synthesis, Characterization and Photocatalytic Performance of Transition Metal Tungstates. *Chem. Phys. Lett.* **2010**, *498*, 113−119.

(24) Lalić, M. V.; Popović, Z. S.; Vukajlović, F. R. Electronic Structure and Optical Properties of $CuWO_4$: An Ab Initio Study. *Comput. Mater. Sci.* **2012**, *63*, 163−167.

DOI: 10.1021/acs.jpclett.7b00664
J. Phys. Chem. Lett. 2017, 8, 2700−2704

(25) Yourey, J. E.; Bartlett, B. M. Electrochemical Deposition and Photoelectrochemistry of $CuWO_4$, a Promising Photoanode for Water Oxidation. *J. Mater. Chem.* **2011**, *21*, 7651−7660.
(26) Hill, J. C.; Choi, K. Synthesis and Characterization of High Surface Area $CuWO_4$ and Bi2WO6 Electrodes for Use as Photoanodes for Solar Water Oxidation. *J. Mater. Chem. A* **2013**, *1*, 5006−5014.
(27) Gao, Y.; Zandi, O.; Hamann, T. W. Atomic Layer Stack Deposition-Annealing Synthesis of $CuWO_4$. *J. Mater. Chem. A* **2016**, *4*, 2826−2830.
(28) Zhang, H.; Yilmaz, P.; Ansari, J. O.; Khan, F. F.; Binions, R.; Krause, S.; Dunn, S. Incorporation of Ag Nanowires in $CuWO_4$ for Improved Visible Light-Induced Photoanode Performance. *J. Mater. Chem. A* **2015**, *3*, 9638−9644.
(29) Pyper, K. J.; Yourey, J. E.; Bartlett, B. M. Reactivity of $CuWO_4$ in Photoelectrochemical Water Oxidation Is Dictated by a Midgap Electronic State. *J. Phys. Chem. C* **2013**, *117*, 24726−24732.
(30) Bohra, D.; Smith, W. A. Improved Charge Separation via Fe-Doping of Copper Tungstate Photoanodes. *Phys. Chem. Chem. Phys.* **2015**, *17*, 9857−9866.
(31) Ye, W.; Chen, F.; Zhao, F.; Han, N.; Li, Y. CuWO4 Nanoflake Array-Based Single-Junction and Heterojunction Photoanodes for Photoelectrochemical Water Oxidation. *ACS Appl. Mater. Interfaces* **2016**, *8*, 9211−9217.
(32) Hu, D.; Diao, P.; Xu, D.; Xia, M.; Gu, Y.; Wu, Q.; Li, C.; Yang, S. Copper (II) Tungstate Nanoflake Array Films: Sacrificial Template Synthesis, Hydrogen Treatment, and Their Application as Photoanodes in Solar Water Splitting. *Nanoscale* **2016**, *8*, 5892−5901.
(33) Gaillard, N.; Chang, Y.; Deangelis, A.; Higgins, S.; Braun, A. A Nanocomposite Photoelectrode Made of 2.2 eV Band Gap Copper Tungstate ($CuWO_4$) and Multi-Wall Carbon Nanotubes for Solar-Assisted Water Splitting. *Int. J. Hydrogen Energy* **2013**, *38*, 3166−3176.
(34) Gao, Y.; Hamann, T. W. Quantitative Hole Collection for Photoelectrochemical Water Oxidation with $CuWO_4$. *Chem. Commun.* **2017**, *53*, 1285−1288.
(35) Klahr, B. M.; Gimenez, S.; Fabregat-santiago, F.; Hamann, T. W.; Bisquert, J. Water Oxidation at Hematite Photoelectrodes: The Role of Surface States. *J. Am. Chem. Soc.* **2012**, *134*, 4294−4302.
(36) Klahr, B. M.; Gimenez, S.; Fabregat-Santiago, F.; Bisquert, J.; Hamann, T. W. Electrochemical and Photoelectrochemical Investigation of Water Oxidation with Hematite Electrodes. *Energy Environ. Sci.* **2012**, *5*, 7626−7636.
(37) Zandi, O.; Hamann, T. W. Determination of Photoelectrochemical Water Oxidation Intermediates on Haematite Electrode Surfaces Using Operando Infrared Spectroscopy. *Nat. Chem.* **2016**, *8*, 778−783.
(38) Klahr, B. M.; Hamann, T. W. Water Oxidation on Hematite Photoelectrodes: Insight into the Nature of Surface States through in Situ Spectroelectrochemistry. *J. Phys. Chem. C* **2014**, *118*, 10393−10399.
(39) Bertoluzzi, L.; Bisquert, J. Equivalent Circuit of Electrons and Holes in Thin Semiconductor Films for Photoelectrochemical Water Splitting Applications. *J. Phys. Chem. Lett.* **2012**, *3*, 2517−2522.
(40) Yourey, J. E.; Pyper, K. J.; Kurtz, J. B.; Bartlett, B. M. Chemical Stability of $CuWO_4$ for Photoelectrochemical Water Oxidation. *J. Phys. Chem. C* **2013**, *117*, 8708−8718.
(41) Bertoluzzi, L.; Badia-bou, L.; Fabregat-santiago, F.; Gimenez, S.; Bisquert, J. Interpretation of Cyclic Voltammetry Measurements of Thin Semiconductor Films for Solar Fuel Applications. *J. Phys. Chem. Lett.* **2013**, *4*, 1334−1339.

DOI: 10.1021/acs.jpclett.7b00664
J. Phys. Chem. Lett. 2017, 8, 2700−2704